

# VTBench: Evaluating Visual Tokenizers for Autoregressive Image Generation

Huawei Lin<sup>1</sup>   Tong Geng<sup>2</sup>   Zhaozhuo Xu<sup>3</sup>   Weijie Zhao<sup>1</sup>

<sup>1</sup> Rochester Institute of Technology   <sup>2</sup> University of Rochester   <sup>3</sup> Stevens Institute of Technology



Code: <https://github.com/huawei-lin/VTBench>



Dataset: <https://huggingface.co/datasets/huaweilin/VTBench>

## Abstract

Autoregressive (AR) models have recently shown strong performance in image generation, where a critical component is the visual tokenizer (VT) that maps continuous pixel inputs to discrete token sequences. The quality of the VT largely defines the upper bound of AR model performance. However, current discrete VTs fall significantly behind continuous variational autoencoders (VAEs), leading to degraded image reconstructions and poor preservation of details and text. Existing benchmarks focus on end-to-end generation quality, without isolating VT performance. To address this gap, we introduce VTBench, a comprehensive benchmark that systematically evaluates VTs across three core tasks: Image Reconstruction, Detail Preservation, and Text Preservation, and covers a diverse range of evaluation scenarios. We systematically assess state-of-the-art VTs using a set of metrics to evaluate the quality of reconstructed images. Our findings reveal that continuous VAEs produce superior visual representations compared to discrete VTs, particularly in retaining spatial structure and semantic detail. In contrast, the degraded representations produced by discrete VTs often lead to distorted reconstructions, loss of fine-grained textures, and failures in preserving text and object integrity. Furthermore, we conduct experiments on GPT-4o image generation and discuss its potential AR nature, offering new insights into the role of visual tokenization. We release our benchmark and codebase publicly to support further research and call on the community to develop strong, general-purpose open-source VTs.

## 1 Introduction

Large Language Models (LLMs) have demonstrated impressive generalization across a wide range of task, including reasoning [29, 33], question answering [54, 38] and text generation [42, 8, 18, 24, 31]. Recent advances suggest that integrating visual understanding and generation into the LLM framework could lead to unified, general-purpose multimodal models [10, 26, 40, 48, 12, 23].

**Visual Tokenizer.** In diffusion-based image generation, images are typically compressed into a continuous latent space using a variational autoencoder (VAE), allowing the model to operate in a lower-dimensional but still continuous domain [15, 34]. However, when integrating visual understanding and generation into LLMs, images must be converted into discrete token sequences, similar to word or subword tokens in natural language processing [9, 3, 44, 25]. Figure 2 illustrates various visual tokenizer architectures and the autoregressive modeling used for image generation.

**Vector Quantized Tokenization.** To enable such tokenization of visual inputs, Vector Quantized Variational Autoencoder (VQ-VAE) is proposed to encode images into a continuous latent space and then map each latent vector to the nearest entry in a learned codebook, producing a discrete index per spatial location [43, 9]. However, scaling the codebook often leads to codebook collapse, where only



Figure 1: Image generation and reconstruction across different models. **(Top)** Images generated from prompts using various models. **(Bottom)** Reconstructions of the GPT-4o-generated chick image using VTs from different models. PSNR  $\uparrow$  values (shown in white) indicates reconstruction fidelity.

a small portion of entries are used, reducing representational capacity. Additionally, nearest-neighbor search introduces computational inefficiency during generation [52, 14]. To address these limitations, Lookup-Free Quantization (LFQ) eliminates the embedding lookup by projecting continuous features into a binary latent space, enabling discrete tokenization without explicit search [52]. To constrain quantization error and enhance stability, Binary Spherical Quantization (BSQ) further introduces  $\ell_2$  normalization during quantization, making the representation smoother and easier to optimize [56].

**Next-Scale Tokenization.** However, AR modeling with existing visual tokenizers often violates the unidirectional dependency assumption and disrupts spatial locality due to the flattening of 2D token grids. To overcome these limitations, Tian et al. [41] proposed Visual Autoregressive Modeling (VAR), which encodes images into multiple levels of tokens by progressively quantizing the residual information at each scale. This hierarchical tokenization preserves spatial structure and allows the model to capture fine-grained details in a coarse-to-fine manner. In Figure 2, we refer to this architecture as "Residual Next-Scale VAE". Building on this foundation, Infinity enhances visual tokenization by integrating BSQ, enabling extremely large vocabularies and efficient scaling. This allows Infinity to generate high-resolution images with unprecedented detail [14].

Despite the growing number of AR models for image generation [22, 2, 47], most existing methods are still limited to relatively simple datasets such as ImageNet and fall significantly behind diffusion models in terms of generation quality and detail preservation. As shown in Figure 1(Top), which presents outputs from several SOTA text-to-image models prompted with highly detailed descriptions, only the images generated by diffusion models (SD3.5L [35] and FLUX.1-dev [20]) and GPT-4o (architecture currently undisclosed [49, 21]) exhibit high-quality synthesis. We hypothesize that the visual tokenizer plays a critical role in this quality gap. To investigate this, we conduct a reconstruction experiment using the images generated by GPT-4o as the ground truth. As shown in Figure 1(Bottom), we reconstruct the chick image using different VTs from various AR models. The results reveal substantial information loss, including blurred text, missing facial features, and structural distortions. These failures indicate that current VTs struggle to generate accurate and expressive latent representations, which limits the overall image generation quality of AR models.

**Why Benchmarking VT Matters?** The reconstruction failures observed in Figure 1 highlight a fundamental issue: current visual tokenizers often fail to preserve fine-grained details and semantic integrity during the quantization process [52, 56]. This failure propagates through the entire AR generation pipeline, ultimately degrading image quality regardless of the downstream model’s capacity. Despite their central role, existing evaluation protocols focus almost exclusively on end-to-end generation quality, without isolating the contribution or limitations of the VT itself. This leaves several critical issues unaddressed: (1) **Lack of VT-Specific Evaluation:** The performance

of the VT often determines the upper bound of AR model quality [52]. Yet, most VTs are only evaluated on limited datasets like ImageNet [36], and there is a lack of dedicated benchmarks designed specifically to measure VT effectiveness across diverse scenarios. (2) **Benchmark Misalignment:** Existing benchmarks evaluate overall image generation (e.g., ImageNet [36], GenEval [13], T2i-compbench [16, 17]), rather than isolating the visual tokenizer contribution, making it difficult to diagnose or improve this key component. (3) **Inadequate Evaluation Metrics:** Commonly used metrics such as FID are insufficient to capture fine-grained failures like high-frequency detail loss or incorrect text reconstruction, which are essential for many multimodal and LLM-centric tasks.

To address these issues, in this paper, we introduce VTBench, a comprehensive benchmark specifically designed to evaluate visual tokenizers across a broad range of tasks, datasets, and conditions. VTBench provides a systematic framework for understanding and improving VTs as standalone components in AR image generation pipelines. Through extensive experiments on a wide range of VTs used in SOTA AR models, we uncover the following key findings: (1) Existing discrete VTs fall significantly behind continuous VAEs used in diffusion models, particularly in terms of reconstruction quality, detail preservation, and text accuracy. (2) None of the existing VTs can robustly handle arbitrary resolutions, unlike continuous VAEs, although VAR [41] and Infinity [14] are restricted to a fixed set of predefined input sizes. (3) Many AR models (e.g., Chameleon [40], Liquid [46], Anole [6]) reuse the same open-source VT, yet there is currently no strong, general-purpose VT available for reuse, highlighting the lack of a reliable, high-quality open-source solution in this space.

**Contributions.** The main contributions of this paper are:

- We introduce VTBench, a high-quality and comprehensive benchmark designed specifically for evaluating VTs in the context of AR image generation.
- We design three tasks: Image Reconstruction, Detail Preservation, and Text Preservation, collectively providing a multi-faceted framework for assessing visual tokenizers. These tasks cover diverse evaluation aspects, including high-resolution inputs, multilingual text scenarios (Chinese, Korean, Japanese, Hindi), and varying-resolution conditions.
- We conduct extensive experiments on VTs used in SOTA AR models, including continuous VAE, GPT4o, VQVAE, etc. Our evaluation is designed to assess both image quality and text preservation through a diverse set of quantitative metrics.
- We provide an in-depth comparison and discussion of current VTs and contrast their behavior with the emerging capabilities of GPT-4o’s VT. We identify fundamental gaps and discuss directions for future tokenizer development.
- We open-source both the codebase and the VTBench dataset to foster further research in visual tokenization for autoregressive image generation. Our codebase is designed to be lightweight and easy to run, requiring minimal setup and no complex configuration.

## 2 Background

In this section, we introduce image generation methods, focusing on both diffusion and AR models. We then discuss the role of visual tokenizers in AR pipelines, reviewing several architectures including VQ-VAE, LFQ-VAE, BSQ-VAE, and Residual Next-Scale VAE, as illustrated in Figure 2. Finally, we highlight recent advances in image generation with GPT-4o, which motivate the need for deeper evaluation of visual tokenization quality.

### 2.1 Image Generation: Diffusion vs. Autoregressive Models

Modern image generation methods are mainly dominated by two families: diffusion models [7, 50] and AR models [11, 4, 53]. Diffusion models learn to iteratively denoise a sample from pure noise to a realistic image using a learned reverse diffusion process, such as Stable Diffusion [35], which have demonstrated SOTA performance in high-quality image synthesis. In contrast, AR models decompose image generation into a sequence modeling problem, where an image is represented as a sequence of discrete tokens predicted one at a time [28, 27, 51], as shown in Figure 2(f). AR models benefit from the scaling properties of LLMs and enable seamless integration with multimodal pipelines. However, AR image generation relies heavily on high-quality visual tokenization to convert pixel data into token sequences and reconstruct images from these tokens, making the design of effective visual tokenizers a central challenge in AR-based image generation.

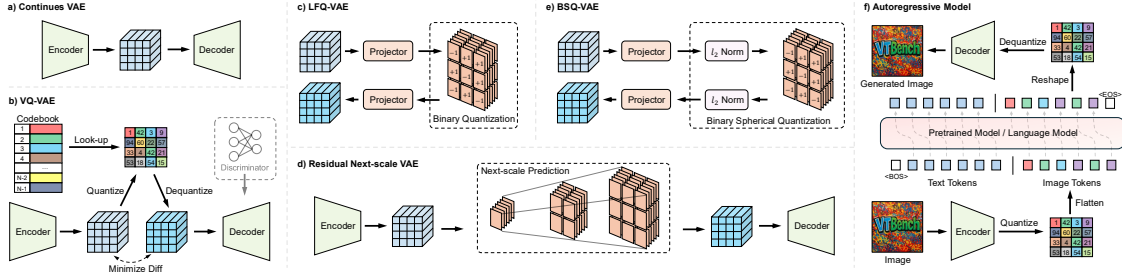


Figure 2: Overview of visual tokenizer architectures and integration with AR image generation.

## 2.2 Visual Tokenizers

To enable AR models to process image inputs, images must be converted into discrete token sequences. This is achieved via visual tokenizers that compress high-dimensional image data into compact, symbolic representations. In this section, we briefly introduce several representative tokenization approaches. We briefly introduce representative tokenization approaches here; a detailed version with mathematical formulations is included in Appendix A.

- **Continuous VAE.** In diffusion models, a common approach is to use a continuous Variational Autoencoder (VAE) [35, 32] as a feature compressor as shown in Figure 2(a). These VAEs encode the input image into a continuous latent space, typically using convolutional encoders and decoders, enabling high-quality image reconstructions.
- **VQ-VAE.** Vector Quantized Variational Autoencoder (VQ-VAE) [43] is one of the earliest and most widely adopted discrete visual tokenizers. It encodes an image into a latent feature map and then quantizes each spatial location to the closest vector in a learned codebook. The resulting discrete indices form a token grid that can be used in AR models.
- **LFQ-VAE.** Lookup-Free Quantization (LFQ) [52] eliminates the nearest-neighbor lookup and codebook by projecting latent features into a binary latent space using a learnable mapping.
- **BSQ-VAE.** Binary Spherical Quantization (BSQ) [56] extends LFQ by applying  $\ell_2$  normalization to the latent features before quantization. This constrains the representation to a unit hypersphere, effectively reducing quantization error and leading to smoother latent spaces. BSQ allows for finer-grained tokenization while maintaining efficient binary encoding, which is beneficial for downstream tasks sensitive to visual detail.
- **Residual Next-Scale VAE.** applies hierarchical tokenization by encoding images in a coarse-to-fine manner. It quantizes residual information across multiple spatial scales, enabling better preservation of structure and fine details, especially in high-resolution settings [41].

## 2.3 GPT-4o Image Generation

OpenAI recently introduced new image generation and editing capabilities in GPT-4o [30], showcasing remarkable performance in both tasks. Although the precise architecture and workflow of GPT-4o remain undisclosed, recent studies suggest that the model may employ an autoregressive backbone in conjunction with a diffusion-based decoder for image synthesis [49, 21]. In this paper, we present extensive experiments on GPT-4o to investigate its underlying architecture and workflow, with a particular focus on how the visual tokenizer influences the quality of generated images.

## 3 VTBench: Task Settings & Evaluation Metrics

To systematically evaluate VTs in AR image generation pipelines, we propose VTBench, a comprehensive benchmark that isolates and diagnoses the capabilities and limitations of VTs across three critical tasks: (1) Image Reconstruction, (2) Detail Preservation, and (3) Text Preservation. Each task is designed to stress different aspects of tokenization quality, using diverse data conditions.

### 3.1 Task 1: Image Reconstruction

This task evaluates the fundamental ability of a VT to reconstruct an image from its tokenized representation. As the interface between high-dimensional pixel inputs and the discrete token



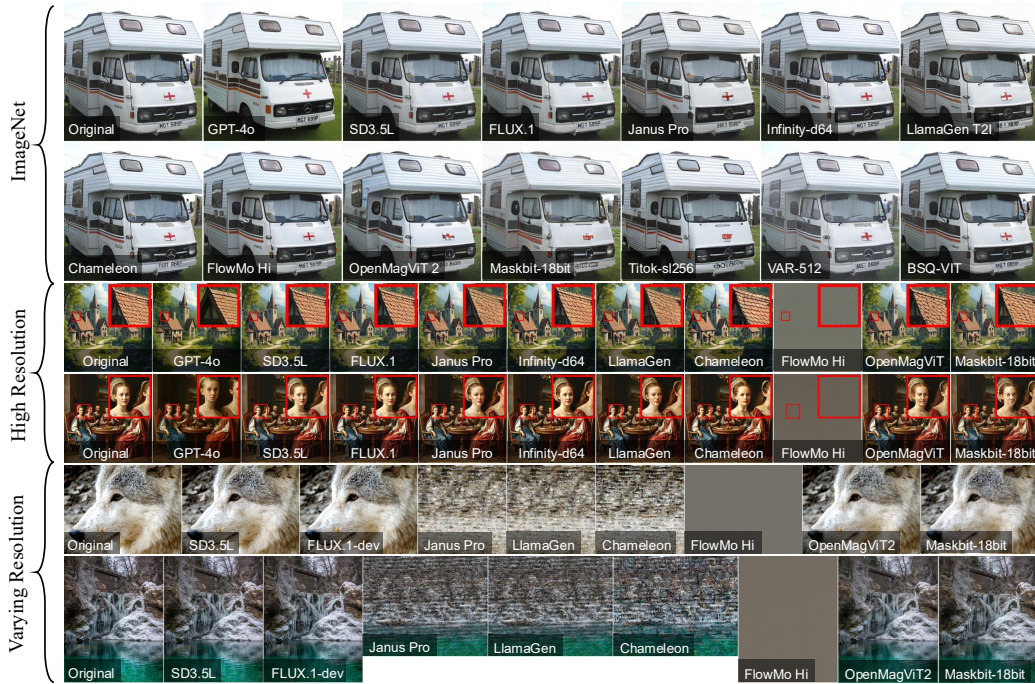


Figure 4: Examples of task 1: (1) ImageNet, (2) High Resolution and (3) Varying Resolution. FlowMo Hi produces corrupted images in High Resolution and Varying Resolution, while Janus Pro, LlamaGen, and Chameleon generate images with incorrect resolution and distorted semantic content.

token representation lacks sufficient expressiveness. A VT that fails to preserve these features will fundamentally limit the quality and realism of generated images. Therefore, this task focuses on measuring how well VTs retain high-frequency information crucial for perceptual fidelity. We follow the same high-resolution synthesis procedure described in Appendix B, using GPT-4o to generate 100 images rich in detailed, high-frequency semantic content.

### 3.3 Task 3: Text Preservation

Text is a uniquely challenging and critical element in many real-world images, especially in domains such as documents, signage, user interfaces, and multimodal reasoning. Unlike general textures, text requires pixel-level precision, minor distortions can render characters unreadable, break words, or alter semantics entirely. Furthermore, text carries symbolic meaning that must be faithfully preserved for models to support language-image alignment, OCR, or instruction-following. However, most VTs are not optimized for symbolic preservation, especially in multilingual or high-density settings. This task evaluates how VTs preserve textual content under varying complexity and linguistic diversity.

**Movie Posters (Easy).** In this subtask, we synthesize 100 images of movie posters. Using GPT-4o, we first generate descriptions for 100 fictional movies along with corresponding slogans, and then produce a poster for each movie. Each poster features a prominent title in large text, a slogan in smaller text, and a background that visually reflects the movie’s theme or genre. Details of synthesis are provided in Appendix B. The dataset spans a wide variety of movie types, providing diverse yet structured visual compositions. A strong VT should preserve both the overall image quality and the legibility of embedded text. Example posters are shown in Figure 3.

**ArXiv Abstracts (Hard).** In addition to the movie posters, we introduce a more challenging subtask consisting of 100 images that render academic paper abstracts. These abstracts feature long sentences, dense layouts, varied font styles, and small font sizes, making this setting particularly demanding. The goal of this task is to evaluate the tokenizer’s ability to preserve fine-grained textual content and maintain layout fidelity under complex visual conditions. To synthesize this dataset, we retrieved abstracts from papers published on April 16, 2025 to ensure that the rendered text images were not included in the training data of any existing VT models.

Table 1: Evaluation of VTs across three reconstruction settings in Task 1.

Method	Params	Type	ImageNet					High Resolution					Varying Resolution			
			Resolution	PSNR $\uparrow$	SSIM $\uparrow$	LPIPS $\downarrow$	FID $\downarrow$	Resolution	PSNR $\uparrow$	SSIM $\uparrow$	LPIPS $\downarrow$	FID $\downarrow$	PSNR $\uparrow$	SSIM $\uparrow$	LPIPS $\downarrow$	FID $\downarrow$
FlowMo Lo	945M	LFQ	256 $\times$ 256	20.2232	0.5878	0.1031	0.8227	1024 $\times$ 1024	11.3631	0.3644	0.6913	465.3528	11.4990	0.2854	0.7379	442.0812
FlowMo Hi	946M	LFQ	256 $\times$ 256	22.4923	0.7103	0.0684	0.4834	1024 $\times$ 1024	11.3077	0.3874	0.6937	439.7494	11.4571	0.2862	0.7353	412.3167
MaskBiT 16bit	54M	LFQ	256 $\times$ 256	19.6448	0.5259	0.1246	1.1473	1024 $\times$ 1024	28.6892	0.9074	0.0313	24.2461	23.9538	0.8037	0.0405	22.4535
MaskBiT 18bit	55M	LFQ	256 $\times$ 256	19.7695	0.5352	0.1197	1.0334	1024 $\times$ 1024	28.9353	0.9135	0.0295	23.3024	23.9289	0.8070	0.0394	23.3959
Titok-i32	641M	VQ	256 $\times$ 256	15.0997	0.3533	0.2922	1.8181	1024 $\times$ 1024	-	-	-	-	-	-	-	-
Titok-b64	204M	VQ	256 $\times$ 256	16.1520	0.3903	0.2285	1.3542	1024 $\times$ 1024	-	-	-	-	-	-	-	-
Titok-s128	83M	VQ	256 $\times$ 256	16.7386	0.4123	0.1898	1.4186	1024 $\times$ 1024	-	-	-	-	-	-	-	-
Titok-b164	390M	VQ	256 $\times$ 256	17.3930	0.4321	0.1926	1.7696	1024 $\times$ 1024	-	-	-	-	-	-	-	-
Titok-bl128	390M	VQ	256 $\times$ 256	18.4675	0.4877	0.1468	1.2328	1024 $\times$ 1024	-	-	-	-	-	-	-	-
Titok-s1256	330M	VQ	256 $\times$ 256	19.6375	0.5514	0.1108	0.8112	1024 $\times$ 1024	-	-	-	-	-	-	-	-
OpenMagViT2	115M	LFQ	256 $\times$ 256	20.0090	0.5786	0.1028	1.0598	1024 $\times$ 1024	30.7770	0.9344	0.0232	18.6649	24.2372	0.8133	0.0383	20.3403
LlamaGen ds8	70M	VQ	256 $\times$ 256	22.4021	0.6995	0.0592	0.4597	1024 $\times$ 1024	33.5435	0.9693	0.0112	10.1195	13.6772	0.2735	0.5401	330.8865
BSQ-ViT	174M	RBS	256 $\times$ 256	<b>25.8646</b>	<b>0.8331</b>	<b>0.0359</b>	<b>0.4586</b>	1024 $\times$ 1024	-	-	-	-	-	-	-	-
VAR-256	109M	RVQ	256 $\times$ 256	20.3693	0.6035	0.0933	0.9080	1024 $\times$ 1024	-	-	-	-	-	-	-	-
Janus Pro 1B/7B	72M	VQ	384 $\times$ 384	22.4485	0.6793	0.0819	0.7111	1024 $\times$ 1024	29.0476	0.9208	0.0299	24.4655	13.1547	0.2342	0.5137	324.0125
Chameleon	68M	VQ	512 $\times$ 512	23.5837	0.7164	0.0672	0.8061	1024 $\times$ 1024	29.3743	0.9062	0.0279	22.6725	12.7700	0.2051	0.5206	331.3999
LlamaGen ds16	72M	VQ	512 $\times$ 512	<b>24.2199</b>	0.7568	<b>0.0630</b>	<b>0.5441</b>	1024 $\times$ 1024	28.6424	0.9148	0.0328	25.0529	13.3258	0.2413	0.5171	327.8920
LlamaGen ds16 T2I	72M	VQ	512 $\times$ 512	24.0192	0.7493	0.0647	0.5528	1024 $\times$ 1024	29.0061	0.9206	0.0300	24.5831	13.1604	0.2344	0.5137	324.4282
VAR-512	109M	RVQ	512 $\times$ 512	22.3828	<b>0.7636</b>	0.0727	0.7719	1024 $\times$ 1024	-	-	-	-	-	-	-	-
Infinity-d32	110M	RBSQ	1024 $\times$ 1024	33.4850	0.9582	0.0109	0.1002	1024 $\times$ 1024	35.5645	0.9732	0.0080	8.3090	-	-	-	-
Infinity-d64	110M	RBSQ	1024 $\times$ 1024	36.0010	0.9766	0.0067	0.0511	1024 $\times$ 1024	37.5937	0.9823	0.0053	5.8734	-	-	-	-
SD3.5L	83M	Continuous	1024 $\times$ 1024	38.8208	0.9836	0.0013	0.0121	1024 $\times$ 1024	38.4653	0.9839	0.0012	0.9787	30.6413	0.9507	0.0075	3.1084
FLUX.1-dev	83M	Continuous	1024 $\times$ 1024	<b>41.6134</b>	<b>0.9932</b>	<b>0.0006</b>	<b>0.0050</b>	1024 $\times$ 1024	<b>41.4870</b>	<b>0.9921</b>	<b>0.0005</b>	<b>0.4466</b>	<b>30.9502</b>	<b>0.9594</b>	<b>0.0068</b>	<b>2.7123</b>
GPT-4o	-	-	1024 $\times$ 1024	19.3828	0.5769	0.1463	39.5056	1024 $\times$ 1024	15.3835	0.4642	0.2077	78.4113	-	-	-	-

**Multilingual (Non-Latin).** To evaluate the cross-lingual robustness of visual tokenizers, we construct a multilingual benchmark consisting of non-Latin scripts, including Chinese, Hindi, Japanese, and Korean. Specifically, we translate the ArXiv abstract texts into each target language using GPT-4o, and then render the translated content into images following the same formatting and layout procedures as in the English version. For each language, we generate 100 text-rich images that reflect real-world typographic complexity. This subtask assesses whether VTs can preserve diverse character sets, linguistic structures, and writing systems that differ significantly from Latin-based scripts.

### 3.4 Evaluation Metrics

To comprehensively evaluate VTs across the three core tasks of VTBench, we adopt a combination of standard and task-specific metrics to capture different dimensions of quality.

**Image Quality.** To assess how well a VT can reconstruct the original image from its tokenized representation, we employ four metrics: (1) **PSNR (Peak Signal-to-Noise Ratio):** Measures pixel-level fidelity between the original and reconstructed images. Higher values indicate better reconstruction. (2) **SSIM (Structural Similarity Index):** Quantifies structural similarity between images by comparing luminance, contrast, and texture. It is more perceptually aligned than PSNR. (3) **LPIPS (Learned Perceptual Image Patch Similarity):** A deep perceptual similarity metric based on features extracted from pretrained networks [55]. It correlates well with human judgment of perceptual quality. (4) **FID (Fréchet Inception Distance):** Measures the distributional distance between real and reconstructed images in the feature space of an Inception network. Lower FID indicates higher quality.

**Text Quality.** Preserving text in images is critical for multimodal reasoning and OCR-related tasks. To quantify this, we apply OCR to the reconstructed images and compare the results to the OCR result of the original image using: (1) **CER (Character Error Rate):** The Levenshtein distance between predicted and ground truth characters, normalized by total character count. (2) **WER (Word Error Rate):** Similar to CER but computed over word sequences. It is particularly sensitive to segmentation and spelling accuracy. For OCR-based evaluation, we utilize Gemma 3 [19], a SOTA multimodal model, to extract textual content from original images and their reconstructed images to calculate WER and CER. The details of OCR and the evaluation of WER and CER are included in Appendix C.

These metrics allow us to analyze not only how much information is retained by the VT, but also what types of information (structural, perceptual, or symbolic) are lost in the tokenization process.

## 4 Experimental Results & Analysis

**Models.** We evaluate a diverse set of VTs spanning multiple quantization paradigms, including Vector Quantization (VQ), Lookup-Free Quantization (LFQ), Binary Spherical Quantization (BSQ), Residual Vector Quantization (RVQ), and Residual Binary Spherical Quantization (RBSQ). Our benchmark covers a wide range of SOTA models such as FlowMo [37], MaskBiT [45], Titok [53], OpenMagViT2 [27], LlamaGen [39], BSQ-ViT [56], VAR [41], Janus Pro [5], Chameleon [40], and



Figure 5: Visualize qualitative results of detail preservation and text preservation.

Infinity [14]. In our experiments, we specifically evaluate the VT component in isolation, without modifying or including the downstream generation models. This design choice allows us to focus purely on the tokenizer’s ability to preserve visual information. For comparison, we also include continuous VAEs used in diffusion models (e.g., SD3.5L [35], FLUX.1-dev [20]) and provide results from GPT-4o [30] as a reference, although its tokenizer architecture remains undisclosed [49]. For GPT-4o, we use the prompt “Please recreate the exact same image without any alterations and preserve the original resolution.” to reconstruct images. Table 1 summarizes all evaluated models along with their parameter counts and quantization types. Additionally, we report the detailed experimental settings and environments in Appendix D.

#### 4.1 Task 1: Image Reconstruction

In this task, we evaluate image reconstruction across three subtasks: (1) ImageNet: Images are center-cropped and resized to match each model’s required input size. (2) High Resolution: All images are set to a fixed size of  $1024 \times 1024$ , and we retain this resolution for all models without resizing. (3) Varying Resolution: This subset contains images with diverse, non-uniform resolutions, and we preserve their original sizes for evaluation. We assess reconstruction quality using PSNR, SSIM, LPIPS, and FID. The results, presented in Table 1, reveal a substantial performance gap between all discrete visual tokenizers and continuous VAEs, with the latter consistently achieving better fidelity and perceptual quality. Notably, results from the High Resolution and Varying Resolution settings highlight that most VTs are limited to model-specific input sizes and fail to generalize to arbitrary resolutions, unlike continuous VAEs, which naturally support flexible image dimensions.

Figure 4 presents qualitative examples illustrating reconstruction quality across different VTs. We observe consistent semantic degradations in discrete VT outputs. For example, red crosses on ambulances are missing or blurred (ImageNet), rooftops are distorted, and facial details, and expressions are noticeably altered (High Resolution). In the Varying Resolution, background textures and object boundaries become heavily corrupted. While models such as Janus Pro, LlamaGen, Chameleon, and FlowMo do not raise runtime errors, they fail to generate correct semantic content, highlighting the inherent limitations of current VTs, especially under high or non-regular resolutions.

Table 3: Evaluation of task 3 across three different settings.

Method	Image Size	Movie Posters (Easy)						ArXiv Abstracts (Hard)						Multilingual (Non-Latin)							
		PSNR $\uparrow$	SSIM $\uparrow$	LPIPS $\downarrow$	FID $\downarrow$	CER $\downarrow$	WER $\downarrow$	PSNR $\uparrow$	SSIM $\uparrow$	LPIPS $\downarrow$	FID $\downarrow$	CER $\downarrow$	WER $\downarrow$	PSNR $\uparrow$	SSIM $\uparrow$	LPIPS $\downarrow$	FID $\downarrow$	CER $\downarrow$ (Chinese)	CER $\downarrow$ (Hindi)	CER $\downarrow$ (Japanese)	CER $\downarrow$ (Korean)
FlowMo Lo	256 $\times$ 256	24.1178	0.7471	0.0645	55.0685	0.6458	3.7022	14.4979	0.5961	0.0703	9.1933	0.8337	6.0968	13.3470	0.5694	0.1187	23.0079	1.2564	1.0397	1.3614	1.2823
FlowMo Hi	256 $\times$ 256	27.4186	0.8403	0.0380	40.7009	0.4169	2.5639	15.8510	0.7262	0.0493	6.6921	0.7046	5.3013	14.4191	0.6932	0.0896	11.8131	1.1279	0.9574	1.0281	0.9981
MaskBIT 16bit	256 $\times$ 256	21.0962	0.6748	0.0992	67.3479	0.7315	4.2234	14.3909	0.4616	0.1945	27.9940	1.3801	9.2146	13.2834	0.4157	0.3184	42.6548	3.1298	1.1953	2.0821	2.1311
MaskBIT 18bit	256 $\times$ 256	21.2932	0.6876	0.0928	64.0766	0.7910	4.8894	14.7015	0.4978	0.2436	26.2086	1.2828	9.2956	13.4963	0.4450	0.3450	59.1847	3.4889	1.1867	1.9445	2.3713
TiTok-I32	256 $\times$ 256	15.5164	0.4595	0.2616	124.7412	1.2254	7.8547	12.2423	0.2390	0.2513	60.0889	1.1178	8.5836	11.6064	0.2440	0.3557	78.3890	3.0154	1.1907	1.9135	1.7847
TiTok-b64	256 $\times$ 256	16.9423	0.5273	0.1939	101.7892	1.0189	6.7070	12.9500	0.3068	0.2470	49.4931	1.2414	10.0394	11.7051	0.2557	0.3163	82.9833	3.5650	1.4384	2.0044	2.3986
TiTok-s128	256 $\times$ 256	17.0506	0.5427	0.1598	88.7466	1.2478	6.2260	12.9276	0.3297	0.2691	56.6373	1.4054	8.6644	11.7860	0.2710	0.3131	64.4152	2.7573	1.1329	1.6614	1.9083
TiTok-b164	256 $\times$ 256	18.2597	0.5963	0.1584	95.2880	1.1421	6.7044	13.4414	0.4535	0.1398	26.4375	1.2385	9.9727	12.1882	0.3908	0.1801	38.8779	3.6473	1.2105	2.8315	2.5622
TiTok-b128	256 $\times$ 256	19.8102	0.6502	0.1159	77.7980	1.5956	5.0851	13.5015	0.4810	0.1235	24.1506	1.0432	7.6730	12.5783	0.4306	0.2012	36.9834	2.3695	0.9719	2.1597	1.8533
TiTok-s1256	256 $\times$ 256	21.4568	0.7151	0.0841	61.0830	0.7850	4.5561	13.4954	0.4996	0.1122	19.0590	1.2131	8.2139	12.7078	0.4669	0.1589	26.0457	2.2980	1.2338	1.9775	1.7088
OpenMagViT	256 $\times$ 256	22.5337	0.7440	0.0741	52.7153	0.7385	4.2419	13.6459	0.5472	0.0900	19.0211	1.0400	7.7046	12.3496	0.4874	0.1498	25.5786	2.5913	1.1622	2.0300	1.9826
LlamaGen ds8	256 $\times$ 256	26.0990	0.8288	0.0371	31.4534	0.5066	2.9620	16.0494	0.7003	0.0648	25.1991	0.9769	7.1170	14.5250	0.6513	0.1024	19.2362	1.1408	1.0250	1.0505	1.1342
BSQ-ViT	256 $\times$ 256	<b>30.7305</b>	<b>0.9135</b>	<b>0.0172</b>	<b>25.6235</b>	<b>0.1102</b>	<b>0.5763</b>	<b>20.3628</b>	<b>0.8910</b>	<b>0.0270</b>	<b>4.7719</b>	<b>0.0459</b>	<b>0.3234</b>	<b>17.9849</b>	<b>0.8544</b>	<b>0.0582</b>	<b>10.2721</b>	<b>0.7858</b>	<b>0.4722</b>	<b>0.3827</b>	<b>0.5919</b>
VAR-256	256 $\times$ 256	23.6215	0.7349	0.0602	50.2971	0.6391	3.7266	15.2481	0.6799	0.0569	23.1849	1.0170	7.3612	13.1452	0.5672	0.1165	19.0211	2.3378	1.1118	1.8972	1.5754
Janus Pro 1B/7B	384 $\times$ 384	25.2793	0.8203	0.0545	45.4080	0.6628	3.7549	17.0286	0.6535	0.1003	38.3604	1.0645	7.8280	15.7220	0.6223	0.1367	53.0056	1.5413	1.1578	1.3463	1.3333
Chameleon	512 $\times$ 512	27.1939	0.8358	0.0430	39.8786	0.5782	3.1359	18.1545	0.7503	0.0588	8.1713	0.7158	5.1867	15.3719	0.6370	0.0977	<b>15.5254</b>	1.9706	0.9171	1.5444	1.4047
LlamaGen ds16	512 $\times$ 512	27.3778	<b>0.8717</b>	0.0440	40.9660	0.4914	2.8774	19.0951	0.7601	0.0601	18.1659	0.9527	6.8741	17.2316	0.7068	0.1141	38.2967	1.2307	1.0938	1.0343	1.1108
LlamaGen ds16 T2I	512 $\times$ 512	<b>27.4929</b>	0.8697	<b>0.0411</b>	<b>38.2986</b>	0.4842	2.5741	18.8911	0.7735	0.0567	20.8214	0.9010	6.1850	17.2267	0.7400	<b>0.0869</b>	45.0646	0.9993	1.0305	0.8139	0.9775
VAR-512	512 $\times$ 512	26.4574	0.8331	0.0486	46.6674	<b>0.1949</b>	<b>1.1867</b>	<b>21.0023</b>	<b>0.8561</b>	<b>0.0553</b>	<b>5.3145</b>	<b>0.1341</b>	<b>0.9829</b>	<b>17.7790</b>	<b>0.7687</b>	0.1012	22.1121	<b>0.8398</b>	<b>0.6873</b>	<b>0.6552</b>	<b>0.7067</b>
Infinity-d32	1024 $\times$ 1024	37.7533	0.9669	0.0063	10.5845	0.0790	0.4371	31.7028	0.9896	0.0049	0.7982	0.0017	0.0162	30.2736	0.9892	0.0086	2.2108	0.1758	0.3552	0.0661	0.0924
Infinity-d64	1024 $\times$ 1024	39.3334	0.9774	0.0048	8.6894	0.0439	0.2978	35.0924	0.9952	0.0026	0.7426	0.0019	0.0165	34.5168	0.9959	0.0035	1.1291	0.1372	0.0604	0.0617	0.0582
SD3.5L	1024 $\times$ 1024	38.9058	0.9650	0.0011	1.6215	<b>0.0002</b>	<b>0.0000</b>	40.1536	0.9988	0.0005	0.1331	<b>0.0001</b>	<b>0.0010</b>	39.6703	0.9989	0.0011	0.4205	<b>0.0973</b>	0.0310	0.1047	0.0545
FLUX.1-dev	1024 $\times$ 1024	<b>44.3863</b>	<b>0.9862</b>	<b>0.0005</b>	<b>0.8993</b>	0.0521	0.4872	<b>52.1000</b>	<b>0.9999</b>	<b>0.0001</b>	<b>0.0256</b>	0.0018	0.0112	<b>51.9243</b>	<b>0.9999</b>	<b>0.0001</b>	<b>0.0457</b>	<b>0.1220</b>	<b>0.0272</b>	<b>0.0614</b>	<b>0.0506</b>
GPT-4o	1024 $\times$ 1024	17.7677	0.6006	0.1388	63.7351	0.0180	0.0836	11.3299	0.1516	0.1929	32.5382	0.4928	3.5292	10.4376	0.1761	0.2291	20.0185	0.8096	0.6414	0.7219	0.6478

## 4.2 Task 2: Detail Preservation

In this task, we evaluate the ability of each VT to retain high-frequency visual information using a dataset of patterned and texture-rich images. As shown in Table 2, continuous VAEs again lead in all metrics. Among discrete VTs, Infinity-d64 demonstrate the strongest performance, suggesting that residual spherical normalization are effective for preserving detailed structures. We further visualize qualitative results in Figure 5. While continuous models such as SD3.5L, and FLUX.1 closely resemble the original, many VTs introduce visible distortions, such as blurred lines, broken shapes, and color bleeding. These results highlight the limitations of current discrete tokenization schemes in retaining local textures and structural integrity.

## 4.3 Task 3: Text Preservation

This task evaluates how well VTs preserve text content in images – a crucial capability for OCR, document understanding, and multimodal reasoning. We consider three increasingly challenging scenarios: (1) Movie Posters with clean, short English text; (2) ArXiv Abstracts containing dense, long-form academic writing; and (3) Multilingual Text rendered in non-Latin scripts (Chinese, Hindi, Japanese, Korean). We use Character Error Rate (CER) and Word Error Rate (WER), based on OCR outputs from the Gemma 3 model, to quantify text preservation. As shown in Table 3 and Figure 5, continuous VAEs such as FLUX.1-dev and SD3.5L consistently outperform discrete tokenizers across all conditions. Notably, many VTs fail to reconstruct even basic slogans or titles in the Movie Poster setting, and perform even worse on dense academic layouts or multilingual scripts. These results highlight the limitations of current discrete tokenization methods in preserving symbolic fidelity, particularly under complex formatting and linguistic diversity.

## 5 Discussion

**Limitation of Existing VTs.** Discrete VTs fall significantly behind continuous VAEs in reconstruction fidelity, detail preservation, and symbolic accuracy, particularly for high-resolution, variable-size, and multilingual inputs. Many models are constrained by fixed input sizes and struggle to retain semantic structure in complex settings. Moreover, the absence of a strong, open-source VT limits progress in large-scale AR models. While LLMs continue to scale and improve, their performance is increasingly bottlenecked by the quality of visual tokenization. There is an urgent need for a resolution-flexible, semantically robust, and reusable VT that can keep pace with the capabilities of modern LLMs. We hope that VTBench can help accelerate research in this direction by providing a unified framework for diagnosis, comparison, and future development.

Table 2: Evaluation of VTs on task 2.

Method	Image Size	PSNR $\uparrow$	SSIM $\uparrow$	LPIPS $\downarrow$	FID $\downarrow$
FlowMo Lo	256 $\times$ 256	17.0642	0.3578	0.1344	64.2895
FlowMo Hi	256 $\times$ 256	19.0346	0.5578	0.0845	44.5536
MaskBIT 16bit	256 $\times$ 256	17.2804	0.2644	0.1803	98.5133
MaskBIT 18bit	256 $\times$ 256	17.3603	0.2728	0.1745	91.3108
TiTok-I32	256 $\times$ 256	15.0325	0.1609	0.3474	169.2162
TiTok-b64	256 $\times$ 256	15.3827	0.1666	0.2767	124.9069
TiTok-s128	256 $\times$ 256	15.6532	0.1828	0.2316	107.7550
TiTok-b164	256 $\times$ 256	15.7606	0.1894	0.2334	121.5447
TiTok-b128	256 $\times$ 256	16.3017	0.2373	0.1808	93.1151
TiTok-s1256	256 $\times$ 256	17.1632	0.3091	0.1413	69.7221
OpenMagViT	256 $\times$ 256	17.0070	0.3278	0.1406	70.6742
LlamaGen ds8	256 $\times$ 256	19.1859	0.5144	0.0852	42.8318
BSQ-ViT	256 $\times$ 256	<b>22.4836</b>	<b>0.7487</b>	<b>0.0496</b>	<b>28.5461</b>
VAR-256	256 $\times$ 256	17.8223	0.3960	0.1207	53.6363
Janus Pro 1B/7B	384 $\times$ 384	20.4726	0.4908	0.1174	59.6669
Chameleon	512 $\times$ 512	20.5686	0.5089	0.1182	67.0157
LlamaGen ds16	512 $\times$ 512	21.8902	0.5903	0.0972	51.3484
LlamaGen ds16 T2I	512 $\times$ 512	<b>21.9694</b>	0.6029	<b>0.0947</b>	<b>51.0251</b>
VAR-512	512 $\times$ 512	21.5492	<b>0.6537</b>	0.1000	57.3488
Infinity-d32	1024 $\times$ 1024	29.1329	0.9052	0.0269	21.0871
Infinity-d64	1024 $\times$ 1024	31.1374	0.9396	0.0188	16.7424
SD3.5L	1024 $\times$ 1024	37.4365	0.9774	0.0028	4.5717
FLUX.1-dev	1024 $\times$ 1024	<b>41.5280</b>	<b>0.9908</b>	<b>0.0011</b>	<b>2.1202</b>
GPT-4o	1024 $\times$ 1024	15.8109	0.3000	0.2156	75.8916

**Insights from GPT-4o Image Generation.** We present additional experiments comparing GPT-4o’s image generation quality with that of diffusion models in Appendix E. The results suggest that GPT-4o may employ an autoregressive generation mechanism, aligning with prior research hypotheses [49]. GPT-4o appears to inherit the knowledge and reasoning capabilities of LLMs while achieving strong visual synthesis quality, indicating its potential as a unified multimodal model. Although the exact architecture of GPT-4o’s VT remains undisclosed, the high quality of its generated images implies a highly capable VT design. Based on qualitative analysis, we hypothesize that GPT-4o may use a residual next-scale VAE (RVAE) [41, 14] or a diffusion-based encoder-decoder [49]. We consider the former more likely, as residual tokenization naturally aligns with the input-output format of LLMs and supports AR generation within a unified framework. This structure would allow the model to seamlessly integrate image understanding and generation, facilitating effective multimodal learning.

## 6 Conclusion

In this paper, we introduce VT Bench, a comprehensive benchmark designed to systematically evaluate the performance of VTs in AR image generation pipelines. Our benchmark spans three tasks: Image Reconstruction, Detail Preservation, and Text Preservation, covering diverse scenarios. Through extensive experiments on a wide range of SOTA VTs, we uncover that discrete VTs fall substantially behind continuous VAEs, particularly in reconstruction fidelity, symbolic accuracy, and spatial consistency. These limitations are further magnified under complex visual conditions. By providing a unified evaluation framework, VT Bench aims to bridge the gap between visual and language modalities, encourage the development of strong open-source VTs, and support the broader goal of building unified, multimodal generative algorithms.

## References

- [1] Eirikur Agustsson and Radu Timofte. Ntire 2017 challenge on single image super-resolution: Dataset and study. In *The IEEE Conference on Computer Vision and Pattern Recognition (CVPR) Workshops*, July 2017.
- [2] Fengxiang Bie, Yibo Yang, Zhongzhu Zhou, Adam Ghanem, Minjia Zhang, Zhewei Yao, Xiaoxia Wu, Connor Holmes, Pareesa Ameneh Golnari, David A. Clifton, Yuxiong He, Dacheng Tao, and Shuaiwen Leon Song. Renaissance: A survey into AI text-to-image generation in the era of large model. *IEEE Trans. Pattern Anal. Mach. Intell.*, 47(3):2212–2231, 2025.
- [3] Huiwen Chang, Han Zhang, Lu Jiang, Ce Liu, and William T. Freeman. Maskgit: Masked generative image transformer. In *IEEE/CVF Conference on Computer Vision and Pattern Recognition, CVPR*, pages 11305–11315, New Orleans, LA, 2022.
- [4] Xiaokang Chen, Zhiyu Wu, Xingchao Liu, Zizheng Pan, Wen Liu, Zhenda Xie, Xingkai Yu, and Chong Ruan. Janus-pro: Unified multimodal understanding and generation with data and model scaling. *CoRR*, abs/2501.17811, 2025.
- [5] Xiaokang Chen, Zhiyu Wu, Xingchao Liu, Zizheng Pan, Wen Liu, Zhenda Xie, Xingkai Yu, and Chong Ruan. Janus-pro: Unified multimodal understanding and generation with data and model scaling. *arXiv preprint arXiv:2501.17811*, 2025.
- [6] Ethan Chern, Jiadi Su, Yan Ma, and Pengfei Liu. ANOLE: an open, autoregressive, native large multimodal models for interleaved image-text generation. *CoRR*, abs/2407.06135, 2024.
- [7] Florinel-Alin Croitoru, Vlad Hondru, Radu Tudor Ionescu, and Mubarak Shah. Diffusion models in vision: A survey. *IEEE Trans. Pattern Anal. Mach. Intell.*, 45(9):10850–10869, 2023.
- [8] DeepSeek-AI, Aixin Liu, Bei Feng, Bing Xue, Bingxuan Wang, Bochao Wu, Chengda Lu, Chenggang Zhao, Chengqi Deng, Chenyu Zhang, Chong Ruan, Damai Dai, Daya Guo, Dejian Yang, Deli Chen, Dongjie Ji, Erhang Li, Fangyun Lin, Fucong Dai, Fuli Luo, Guangbo Hao, Guanting Chen, Guowei Li, H. Zhang, Han Bao, Hanwei Xu, Haocheng Wang, Haowei Zhang, Honghui Ding, Huajian Xin, Huazuo Gao, Hui Li, Hui Qu, J. L. Cai, Jian Liang, Jianzhong Guo, Jiaqi Ni, Jiashi Li, Jiawei Wang, Jin Chen, Jingchang Chen, Jingyang Yuan, Junjie Qiu, Junlong Li, Junxiao Song, Kai Dong, Kai Hu, Kaige Gao, Kang Guan, Kexin Huang, Kuai Yu, Lean

- Wang, Lecong Zhang, Lei Xu, Leyi Xia, Liang Zhao, Litong Wang, Liyue Zhang, Meng Li, Miaojun Wang, Mingchuan Zhang, Minghua Zhang, Minghui Tang, Mingming Li, Ning Tian, Panpan Huang, Peiyi Wang, Peng Zhang, Qiancheng Wang, Qihao Zhu, Qinyu Chen, Qiushi Du, R. J. Chen, R. L. Jin, Ruiqi Ge, Ruisong Zhang, Ruizhe Pan, Runji Wang, Runxin Xu, Ruoyu Zhang, Ruyi Chen, S. S. Li, Shanghao Lu, Shangyan Zhou, Shanhuang Chen, Shaoqing Wu, Shengfeng Ye, Shengfeng Ye, Shirong Ma, Shiyu Wang, Shuang Zhou, Shuiping Yu, Shunfeng Zhou, Shuting Pan, T. Wang, Tao Yun, Tian Pei, Tianyu Sun, W. L. Xiao, and Wangding Zeng. Deepseek-v3 technical report. *CoRR*, abs/2412.19437, 2024.
- [9] Patrick Esser, Robin Rombach, and Björn Ommer. Taming transformers for high-resolution image synthesis. In *IEEE Conference on Computer Vision and Pattern Recognition, CVPR*, pages 12873–12883, virtual, 2021. Computer Vision Foundation / IEEE.
- [10] Lijie Fan, Tianhong Li, Siyang Qin, Yuanzhen Li, Chen Sun, Michael Rubinstein, Deqing Sun, Kaiming He, and Yonglong Tian. Fluid: Scaling autoregressive text-to-image generative models with continuous tokens. *CoRR*, abs/2410.13863, 2024.
- [11] Lijie Fan, Luming Tang, Siyang Qin, Tianhong Li, Xuan Yang, Siyuan Qiao, Andreas Steiner, Chen Sun, Yuanzhen Li, Tao Zhu, Michael Rubinstein, Michalis Raptis, Deqing Sun, and Radu Soricut. Unified autoregressive visual generation and understanding with continuous tokens. *CoRR*, abs/2503.13436, 2025.
- [12] Yuying Ge, Sijie Zhao, Jinguo Zhu, Yixiao Ge, Kun Yi, Lin Song, Chen Li, Xiaohan Ding, and Ying Shan. SEED-X: multimodal models with unified multi-granularity comprehension and generation. *CoRR*, abs/2404.14396, 2024.
- [13] Dhruva Ghosh, Hannaneh Hajishirzi, and Ludwig Schmidt. Geneval: An object-focused framework for evaluating text-to-image alignment. In *Advances in Neural Information Processing Systems NeurIPS*, New Orleans, LA, 2023.
- [14] Jian Han, Jinlai Liu, Yi Jiang, Bin Yan, Yuqi Zhang, Zehuan Yuan, Bingyue Peng, and Xiaobing Liu. Infinity: Scaling bitwise autoregressive modeling for high-resolution image synthesis. *CoRR*, abs/2412.04431, 2024.
- [15] Jonathan Ho, Ajay Jain, and Pieter Abbeel. Denoising diffusion probabilistic models. In *Advances in Neural Information Processing Systems NeurIPS*, virtual, 2020.
- [16] Kaiyi Huang, Kaiyue Sun, Enze Xie, Zhenguo Li, and Xihui Liu. T2i-compbench: A comprehensive benchmark for open-world compositional text-to-image generation. In *Advances in Neural Information Processing Systems NeurIPS*, New Orleans, LA, 2023.
- [17] Kaiyi Huang, Chengqi Duan, Kaiyue Sun, Enze Xie, Zhenguo Li, and Xihui Liu. T2i-compbench++: An enhanced and comprehensive benchmark for compositional text-to-image generation. *IEEE Trans. Pattern Anal. Mach. Intell.*, 47(5):3563–3579, 2025.
- [18] Albert Q. Jiang, Alexandre Sablayrolles, Antoine Roux, Arthur Mensch, Blanche Savary, Chris Bamford, Devendra Singh Chaplot, Diego de Las Casas, Emma Bou Hanna, Florian Bressand, Gianna Lengyel, Guillaume Bour, Guillaume Lample, L  lio Renard Lavaud, Lucile Saulnier, Marie-Anne Lachaux, Pierre Stock, Sandeep Subramanian, Sophia Yang, Szymon Antoniak, Teven Le Scao, Th  ophile Gervet, Thibaut Lavril, Thomas Wang, Timoth  e Lacroix, and William El Sayed. Mixtral of experts. *CoRR*, abs/2401.04088, 2024.
- [19] Aishwarya Kamath, Johan Ferret, Shreya Pathak, Nino Vieillard, Ramona Merhej, Sarah Perrin, Tatiana Matejovicova, Alexandre Ram  , Morgane Rivi  re, Louis Rouillard, Thomas Mesnard, Geoffrey Cideron, Jean-Bastien Grill, Sabela Ramos, Edouard Yvinec, Michelle Casbon, Etienne Pot, Ivo Penchev, Ga  l Liu, Francesco Visin, Kathleen Kenealy, Lucas Beyer, Xiaohai Zhai, Anton Tsitsulin, R  bert Busa-Fekete, Alex Feng, Noveen Sachdeva, Benjamin Coleman, Yi Gao, Basil Mustafa, Iain Barr, Emilio Parisotto, David Tian, Matan Eyal, Colin Cherry, Jan-Thorsten Peter, Danila Sinopalnikov, Surya Bhupatiraju, Rishabh Agarwal, Mehran Kazemi, Dan Malkin, Ravin Kumar, David Vilar, Idan Brusilovsky, Jiaming Luo, Andreas Steiner, Abe Friesen, Abhanshu Sharma, Abheesht Sharma, Adi Mayrav Gilady, Adrian Goedeckemeyer, Alaa Saade, Alexander Kolesnikov, Alexei Bendebury, Alvin Abdagic, Amit Vadi, Andr  s

- György, André Susano Pinto, Anil Das, Ankur Bapna, Antoine Miech, Antoine Yang, Antonia Paterson, Ashish Shenoy, Ayan Chakrabarti, Bilal Piot, Bo Wu, Bobak Shahriari, Bryce Pettrini, Charlie Chen, Charline Le Lan, Christopher A. Choquette-Choo, CJ Carey, Cormac Brick, Daniel Deutsch, Danielle Eisenbud, Dee Cattle, Derek Cheng, Dimitris Paparas, Divyashree Shivakumar Sreepathihalli, Doug Reid, Dustin Tran, Dustin Zelle, Eric Noland, Erwin Huizenga, Eugene Kharitonov, Frederick Liu, Gagik Amirkhanyan, Glenn Cameron, Hadi Hashemi, Hanna Klimczak-Plucinska, Harman Singh, Harsh Mehta, Harshal Tushar Lehri, Hussein Hazimeh, Ian Ballantyne, Idan Szpektor, and Ivan Nardini. Gemma 3 technical report. *CoRR*, abs/2503.19786, 2025.
- [20] Black Forest Labs. Flux. <https://github.com/black-forest-labs/flux>, 2024.
- [21] Ning Li, Jingran Zhang, and Justin Cui. Have we unified image generation and understanding yet? an empirical study of gpt-4o’s image generation ability. *arXiv preprint arXiv:2504.08003*, 2025.
- [22] Tianhong Li, Yonglong Tian, He Li, Mingyang Deng, and Kaiming He. Autoregressive image generation without vector quantization. In *Advances in Neural Information Processing Systems NeurIPS*, Vancouver, BC, Canada, 2024.
- [23] Huawei Lin, Yingjie Lao, and Weijie Zhao. Dmin: Scalable training data influence estimation for diffusion models. *CoRR*, abs/2412.08637, 2024.
- [24] Huawei Lin, Jikai Long, Zhaozhuo Xu, and Weijie Zhao. Token-wise influential training data retrieval for large language models. In *Proceedings of the 62nd Annual Meeting of the Association for Computational Linguistics (Volume 1: Long Papers)*, *ACL*, pages 841–860, Bangkok, Thailand, 2024. Association for Computational Linguistics.
- [25] Huawei Lin, Yingjie Lao, Tong Geng, Tan Yu, and Weijie Zhao. Uniguards: A unified defense for detecting prompt injection, backdoor attacks and adversarial attacks in large language models. *CoRR*, abs/2502.13141, 2025.
- [26] Jiasen Lu, Christopher Clark, Sangho Lee, Zichen Zhang, Savva Khosla, Ryan Marten, Derek Hoiem, and Aniruddha Kembhavi. Unified-io 2: Scaling autoregressive multimodal models with vision, language, audio, and action. In *IEEE/CVF Conference on Computer Vision and Pattern Recognition, CVPR 2024, USA, June 16-22, 2024*, pages 26429–26445, Seattle, WA, 2024.
- [27] Zhuoyan Luo, Fengyuan Shi, Yixiao Ge, Yujiu Yang, Limin Wang, and Ying Shan. Openmagvit2: An open-source project toward democratizing auto-regressive visual generation. *CoRR*, abs/2409.04410, 2024.
- [28] Xu Ma, Peize Sun, Haoyu Ma, Hao Tang, Chih-Yao Ma, Jialiang Wang, Kunpeng Li, Xiaoliang Dai, Yujun Shi, Xuan Ju, et al. Token-shuffle: Towards high-resolution image generation with autoregressive models. *arXiv preprint arXiv:2504.17789*, 2025.
- [29] Xuefei Ning, Zifu Wang, Shiyao Li, Zinan Lin, Peiran Yao, Tianyu Fu, Matthew B. Blaschko, Guohao Dai, Huazhong Yang, and Yu Wang. Can llms learn by teaching for better reasoning? A preliminary study. In *Advances in Neural Information Processing Systems, NeurIPS*, Vancouver, BC, Canada, 2024.
- [30] OpenAI. Introducing 4o image generation, 2025. URL <https://openai.com/index/introducing-4o-image-generation/>.
- [31] Yanzhou Pan, Huawei Lin, Yide Ran, Jiamin Chen, Xiaodong Yu, Weijie Zhao, Denghui Zhang, and Zhaozhuo Xu. Alinfik: Learning to approximate linearized future influence kernel for scalable third-parity LLM data valuation. *CoRR*, abs/2503.01052, 2025.
- [32] William Peebles and Saining Xie. Scalable diffusion models with transformers. In *IEEE/CVF International Conference on Computer Vision, ICCV*, pages 4172–4182, Paris, France, 2023.
- [33] Aske Plaat, Annie Wong, Suzan Verberne, Joost Broekens, Niki van Stein, and Thomas Bäck. Reasoning with large language models, a survey. *CoRR*, abs/2407.11511, 2024.

- [34] Robin Rombach, Andreas Blattmann, Dominik Lorenz, Patrick Esser, and Björn Ommer. High-resolution image synthesis with latent diffusion models. *CoRR*, abs/2112.10752, 2021.
- [35] Robin Rombach, Andreas Blattmann, Dominik Lorenz, Patrick Esser, and Björn Ommer. High-resolution image synthesis with latent diffusion models. In *IEEE/CVF Conference on Computer Vision and Pattern Recognition, CVPR*, pages 10674–10685, New Orleans, LA, 2022.
- [36] Olga Russakovsky, Jia Deng, Hao Su, Jonathan Krause, Sanjeev Satheesh, Sean Ma, Zhiheng Huang, Andrej Karpathy, Aditya Khosla, Michael S. Bernstein, Alexander C. Berg, and Li Fei-Fei. Imagenet large scale visual recognition challenge. *Int. J. Comput. Vis.*, 115(3):211–252, 2015.
- [37] Kyle Sargent, Kyle Hsu, Justin Johnson, Li Fei-Fei, and Jiajun Wu. Flow to the mode: Mode-seeking diffusion autoencoders for state-of-the-art image tokenization. *CoRR*, abs/2503.11056, 2025.
- [38] Chonghao Sima, Katrin Renz, Kashyap Chitta, Li Chen, Hanxue Zhang, Chengen Xie, Jens Beißwenger, Ping Luo, Andreas Geiger, and Hongyang Li. Drivelm: Driving with graph visual question answering. In *Computer Vision - ECCV 2024 - 18th European Conference, Milan, Italy, September 29-October 4, 2024, Proceedings, Part LII*, volume 15110 of *Lecture Notes in Computer Science*, pages 256–274, 2024.
- [39] Peize Sun, Yi Jiang, Shoufa Chen, Shilong Zhang, Bingyue Peng, Ping Luo, and Zehuan Yuan. Autoregressive model beats diffusion: Llama for scalable image generation. *CoRR*, abs/2406.06525, 2024.
- [40] Chameleon Team. Chameleon: Mixed-modal early-fusion foundation models. *CoRR*, abs/2405.09818, 2024.
- [41] Keyu Tian, Yi Jiang, Zehuan Yuan, Bingyue Peng, and Liwei Wang. Visual autoregressive modeling: Scalable image generation via next-scale prediction. In *Advances in Neural Information Processing Systems 38: Annual Conference on Neural Information Processing Systems, NeurIPS*, Vancouver, BC, Canada, 2024.
- [42] Hugo Touvron, Thibaut Lavril, Gautier Izacard, Xavier Martinet, Marie-Anne Lachaux, Timothée Lacroix, Baptiste Rozière, Naman Goyal, Eric Hambro, Faisal Azhar, Aurélien Rodriguez, Armand Joulin, Edouard Grave, and Guillaume Lample. Llama: Open and efficient foundation language models. *CoRR*, abs/2302.13971, 2023.
- [43] Aäron van den Oord, Oriol Vinyals, and Koray Kavukcuoglu. Neural discrete representation learning. In *Advances in Neural Information Processing Systems 30: Annual Conference on Neural Information Processing Systems 2017, December 4-9, 2017, Long Beach, CA, USA*, pages 6306–6315, Long Beach, CA, 2017.
- [44] Guangzhi Wang, Yixiao Ge, Xiaohan Ding, Mohan S. Kankanhalli, and Ying Shan. What makes for good visual tokenizers for large language models? *CoRR*, abs/2305.12223, 2023.
- [45] Mark Weber, Lijun Yu, Qihang Yu, Xueqing Deng, Xiaohui Shen, Daniel Cremers, and Liang-Chieh Chen. Maskbit: Embedding-free image generation via bit tokens. *CoRR*, abs/2409.16211, 2024.
- [46] Junfeng Wu, Yi Jiang, Chuofan Ma, Yuliang Liu, Hengshuang Zhao, Zehuan Yuan, Song Bai, and Xiang Bai. Liquid: Language models are scalable multi-modal generators. *arXiv preprint arXiv:2412.04332*, 2024.
- [47] Yecheng Wu, Zhuoyang Zhang, Junyu Chen, Haotian Tang, Dacheng Li, Yunhao Fang, Ligeng Zhu, Enze Xie, Hongxu Yin, Li Yi, Song Han, and Yao Lu. VILA-U: a unified foundation model integrating visual understanding and generation. *CoRR*, abs/2409.04429, 2024.
- [48] Jinheng Xie, Weijia Mao, Zechen Bai, David Junhao Zhang, Weihao Wang, Kevin Qinghong Lin, Yuchao Gu, Zhijie Chen, Zhenheng Yang, and Mike Zheng Shou. Show-o: One single transformer to unify multimodal understanding and generation. *CoRR*, abs/2408.12528, 2024.

- [49] Zhiyuan Yan, Junyan Ye, Weijia Li, Zilong Huang, Shenghai Yuan, Xiangyang He, Kaiqing Lin, Jun He, Conghui He, and Li Yuan. Gpt-imgeval: A comprehensive benchmark for diagnosing gpt4o in image generation. *arXiv preprint arXiv:2504.02782*, 2025.
- [50] Ling Yang, Zhilong Zhang, Yang Song, Shenda Hong, Runsheng Xu, Yue Zhao, Wentao Zhang, Bin Cui, and Ming-Hsuan Yang. Diffusion models: A comprehensive survey of methods and applications. *ACM Comput. Surv.*, 56(4):105:1–105:39, 2024.
- [51] Lijun Yu, Yong Cheng, Kihyuk Sohn, José Lezama, Han Zhang, Huiwen Chang, Alexander G. Hauptmann, Ming-Hsuan Yang, Yuan Hao, Irfan Essa, and Lu Jiang. MAGVIT: masked generative video transformer. In *IEEE/CVF Conference on Computer Vision and Pattern Recognition, CVPR*, pages 10459–10469, Vancouver, BC, Canada, 2023.
- [52] Lijun Yu, José Lezama, Nitesh Bharadwaj Gundavarapu, Luca Versari, Kihyuk Sohn, David Minnen, Yong Cheng, Agrim Gupta, Xiuye Gu, Alexander G. Hauptmann, Boqing Gong, Ming-Hsuan Yang, Irfan Essa, David A. Ross, and Lu Jiang. Language model beats diffusion - tokenizer is key to visual generation. In *The Twelfth International Conference on Learning Representations, ICLR*, Vienna, Austria, 2024.
- [53] Qihang Yu, Mark Weber, Xueqing Deng, Xiaohui Shen, Daniel Cremers, and Liang-Chieh Chen. An image is worth 32 tokens for reconstruction and generation. In *Advances in Neural Information Processing Systems, NeurIPS*, Vancouver, BC, Canada, 2024.
- [54] Ce Zhang, Taixi Lu, Md Mohaiminul Islam, Ziyang Wang, Shoubin Yu, Mohit Bansal, and Gedas Bertasius. A simple LLM framework for long-range video question-answering. In *Proceedings of the 2024 Conference on Empirical Methods in Natural Language Processing, EMNLP*, pages 21715–21737, Miami, FL, 2024.
- [55] Richard Zhang, Phillip Isola, Alexei A. Efros, Eli Shechtman, and Oliver Wang. The unreasonable effectiveness of deep features as a perceptual metric. In *2018 IEEE Conference on Computer Vision and Pattern Recognition, CVPR*, pages 586–595, Salt Lake City, UT, 2018.
- [56] Yue Zhao, Yuanjun Xiong, and Philipp Krähenbühl. Image and video tokenization with binary spherical quantization. *CoRR*, abs/2406.07548, 2024.

## A Extended Background on Visual Tokenizers

While the main text provides a brief overview of VTs, this section offers a more detailed explanation of representative visual tokenizers, including both continuous and discrete variants. We present formal definitions and architectural insights for each method, laying the groundwork for understanding their differences in performance and suitability for autoregressive image generation.

**Continuous VAE.** In diffusion models, a common approach is to use a continuous Variational Autoencoder (VAE) [35, 32] as a feature compressor as shown in Figure 2(a). These VAEs encode the input image into a continuous latent space, typically using convolutional encoders and decoders, enabling high-quality image reconstructions. Formally, let  $x \in \mathbb{R}^{H \times W \times 3}$  be the input image, where  $H$  and  $W$  denote the image’s height and width, respectively. The encoder  $E$  maps  $x$  to a latent representation  $z = E(x) \in \mathbb{R}^{h \times w \times d}$ , where  $h$  and  $w$  are the spatial dimensions of the latent space (typically downsampled from  $H$  and  $W$ ), and  $d$  is the latent channel dimension. The decoder  $D$  reconstructs the image as  $\hat{x} = D(z)$ . However, AR models require inputs in the form of discrete token sequences, motivating the development of discrete visual tokenizers.

**VQ-VAE.** Vector Quantized Variational Autoencoder (VQ-VAE) [43] is one of the earliest and most widely adopted discrete visual tokenizers. It encodes an image into a latent feature map and then quantizes each spatial location to the closest vector in a learned codebook. The resulting discrete indices form a token grid that can be used in AR models. Given an input image  $x \in \mathbb{R}^{H \times W \times 3}$ , the encoder  $E$  produces a latent map  $z = E(x) \in \mathbb{R}^{h \times w \times d}$ . Each latent vector  $z_{i,j}$  is replaced by its nearest neighbor in the codebook  $\mathcal{C} = \{c_1, c_2, \dots, c_K\} \subset \mathbb{R}^d$ ,  $q_{i,j} = \arg \min_k \|z_{i,j} - c_k\|_2^2$ ,  $\hat{z}_{i,j} = c_{q_{i,j}}$ . The quantized latent  $\hat{z}$  is then decoded via  $D$  to reconstruct the image  $\hat{x} = D(\hat{z})$ . While VQ-VAE enables discrete tokenization suitable for AR models, it suffers from limited expressivity, codebook collapse, and scalability issues when handling high-resolution or diverse image content.

**LFQ-VAE.** Lookup-Free Quantization (LFQ) [52] eliminates the nearest-neighbor lookup and codebook structure by directly projecting latent features into a binary latent space using a learnable mapping. The encoder  $E$  produces  $z = E(x) \in \mathbb{R}^{h \times w \times d}$ . Each element  $z_{i,j,k}$  is quantized using a sign function:  $\hat{z}_{i,j,k} = \text{sign}(z_{i,j,k}) \in \{-1, +1\}$ . The binary representation can be interpreted as a discrete token mask  $m$ , where each binary vector at location  $(i, j)$  is mapped to an integer token using  $m_{i,j} = \sum_{k=1}^d 2^{k-1} \mathbb{1}_{z_{i,j,k} > 0}$ .

**BSQ-VAE.** Binary Spherical Quantization (BSQ) [56] builds upon LFQ by incorporating  $\ell_2$  normalization before quantization:  $\hat{z}_{i,j,k} = \frac{1}{|\sqrt{d}|} \text{sign}\left(\frac{z_{i,j,k}}{|z_{i,j}|}\right)$ . This constrains the representation to a unit hypersphere, effectively reducing quantization error and leading to smoother latent spaces. BSQ allows for finer-grained tokenization while maintaining efficient binary encoding, which is beneficial for downstream tasks sensitive to visual detail.

**Residual Next-Scale VAE** introduces hierarchical tokenization by progressively quantizing residual information across multiple spatial scales [41]. Let  $s \in \{1, 2, \dots, n\}$  denote the scale index, where  $n$  is the total number of scales. Each scale  $s$  corresponds to a predefined spatial resolution  $(h_s, w_s)$ , with  $h_s \leq h$  and  $w_s \leq w$ . During encoding, a sequence of quantized tokens  $\hat{z} = \{\hat{z}^{(1)}, \hat{z}^{(2)}, \dots, \hat{z}^{(n)}\}$  is computed as follows:

$$\begin{cases} z = r^{(0)} = E(x) \in \mathbb{R}^{h \times w \times d} \\ \hat{z}^{(s)} = \mathcal{Q}\left(\downarrow_{(h_s, w_s)}\left(r^{(s-1)}\right)\right), \quad r^{(s)} = z - \uparrow_{(h, w)}\left(\mathcal{D}\left(\hat{z}^{(s)}\right)\right), \quad s = 1, \dots, n \end{cases} \quad (1)$$

Here,  $\mathcal{Q}$  and  $\mathcal{D}$  represent the quantization and dequantization functions, respectively, which may be implemented using VQ, LFQ, BSQ, or similar methods. The operators  $\downarrow_{(h_s, w_s)}(\cdot)$  and  $\uparrow_{(h, w)}(\cdot)$  denote downsampling to and upsampling from the specified resolution. During decoding, the final image is reconstructed by aggregating and decoding all quantized components:

$$\hat{x} = D\left(\sum_{s=1}^n \uparrow_{(h, w)}\left(\mathcal{D}(\hat{z}^{(s)})\right)\right) \quad (2)$$

This coarse-to-fine scheme preserves spatial structure and enables the model to capture both global context and fine-grained details, making it effective for high-resolution image reconstruction.

## B Image Synthesis

In this section, we detail the procedure for synthesizing high-resolution and detailed images.

**High Resolution Images.** To generate diverse scene descriptions, we use the prompt: “*I want to generate high-resolution images with a size of  $1024 \times 1024$ . Please directly create 10 different fictional scenes for me and output them in JSONL format.*” This prompt is repeated 10 times, resulting in 100 unique scene descriptions. Each description is then passed to GPT-4o’s image generation API to produce 100 corresponding images, each with a resolution of  $1024 \times 1024$ .

**Detailed Images.** Following a similar approach to high-resolution image synthesis, we employed the following prompt: “*I want to design a richly detailed dataset, featuring abundant lines, color blocks, textures, or various forms of high-frequency information. The scenes do not need to be realistic. I plan to use image generation algorithms to produce these images. Please help me design 5 different prompts and output them in JSONL format.*” This prompt is issued 10 times to generate a total of 100 unique scene descriptions. Each description is then used with GPT-4o’s image generation API to synthesize 100 corresponding images at a resolution of  $1024 \times 1024$ .

**Movie Poster Synthesis** To synthesize movie posters, we first generate fictional movie titles and subtitles using the prompt: “*Please generate a fictional movie titles of different types, along with subtitles, and output them in JSONL format.*” These synthetic titles and subtitles are then used in a second prompt to create the corresponding posters: “*Generate a  $1024 \times 1024$  movie poster for the film titled (movie title), incorporating the text: (subtitle). The title and slogan should blend naturally into the poster design.*” This process is repeated 100 times to produce 100 unique movie posters.

## C Text Quality Evaluation

Evaluating the ability of a VT to preserve text content is critical for many downstream applications such as OCR, document generation/understanding, and multimodal reasoning. In VTBench, we quantify this ability by applying Optical Character Recognition (OCR) to both original and reconstructed images, and computing standard text similarity metrics based on the OCR outputs.

**Optical Character Recognition (OCR)** We use a SOTA multimodal model, Gemma 3 [19], to extract textual content from both the original image  $x$  and the reconstructed image  $\hat{x}$ . Let  $T_{\text{orig}}$  and  $T_{\text{recon}}$  denote the sequences obtained from  $x$  and  $\hat{x}$ , respectively. All evaluations are performed under the same OCR configuration to ensure consistency.

**Character Error Rate (CER)** The Character Error Rate measures the normalized edit distance between two character sequences. Given the ground-truth sequence  $T_{\text{orig}}$  and the predicted sequence  $T_{\text{recon}}$ , CER is computed as:

$$\text{CER} = \frac{D_{\text{char}}(T_{\text{orig}}, T_{\text{recon}})}{|T_{\text{orig}}|} \quad (3)$$

where  $D_{\text{char}}(\cdot, \cdot)$  denotes the Levenshtein distance (i.e., the minimum number of insertions, deletions, and substitutions needed to convert one character sequence to another), and  $|T_{\text{orig}}|$  is the number of characters in the ground-truth sequence.

**Word Error Rate (WER).** Word Error Rate is similar to CER, but computed at the word level. Let  $W_{\text{orig}}$  and  $W_{\text{recon}}$  be the sequences of words extracted from the original and reconstructed images, respectively. The WER is defined as:

$$\text{WER} = \frac{D_{\text{word}}(W_{\text{orig}}, W_{\text{recon}})}{|W_{\text{orig}}|} \quad (4)$$

where  $D_{\text{word}}(\cdot, \cdot)$  is the Levenshtein distance between word sequences, and  $|W_{\text{orig}}|$  is the number of words in the ground-truth text.

As with CER, WER can also exceed 1 in extreme failure cases, where the number of incorrect or missing words far surpasses the original word count. These metrics jointly capture both low-level character accuracy and higher-level semantic correctness. High CER or WER indicates that the visual tokenizer has failed to preserve text layout or visual clarity during reconstruction, especially in multilingual or high-density text scenarios.

## D Experimental Settings and Environments

**Experimental Settings.** We evaluate a range of SOTA VTs across the three core tasks in VTBench: Image Reconstruction, Detail Preservation, and Text Preservation. For each task, we use a fixed evaluation protocol to ensure consistency across models. All tokenizers are evaluated in an inference-only setting using publicly available pretrained weights. Where applicable, we follow each model’s official preprocessing pipeline and input size specification (see Table 1). For text preservation evaluation, OCR is applied to both original and reconstructed images before computing CER and WER. We use the same set of 50,000 ImageNet validation images and 100 samples per text benchmark (movie posters, abstracts, multilingual) for all models.

**Environments.** All experiments are conducted using 4 NVIDIA A100 80GB GPUs with 251GB memory. Image preprocessing, reconstruction, and OCR evaluation are run on a standardized, reproducible pipeline. All results are collected on the same hardware and software stack to ensure fair comparisons.

## E Additional Experiments of GPT-4o Image Generation

To further understand the GPT-4o’s architecture and VT, we conducted a set of controlled experiments focused on its capabilities in font recognition and fine-grained text editing. These experiments are designed to isolate and probe the internal mechanisms behind GPT-4o’s image generation and editing abilities, specifically evaluating the underlying VT’s expressiveness and semantic alignment.

Original	InstructPix2Pix	Step1X-Edit	IC-Edit	GPT-4o	GPT-4o-OCR (Extract from original image)
					<p>[2023-04-16] We introduce H3Net b1.59 2847: the first open-source, native 3-bit Large Language Model (LLM) at the 2-billion parameter scale. Trained on a corpus of a trillion tokens, the model has been rigorously evaluated across benchmarks covering language understanding, mathematical reasoning, coding proficiency, and conversational ability. Our results demonstrate that H3Net b1.59 2847 achieves performance on par with leading open-weight, full-precision LLMs of similar size, while offering significant advantages in computational efficiency, including substantially reduced memory footprint, energy consumption, and decoding latency. To facilitate further research and adoption, the quantized weights are released via Hugging Face along with open-source reference implementations for both GPU and CPU architectures.</p>
					<p>[2023-04-16] We present a geometry-driven method for normalizing dysarthric speech using local Lie group transformations of spectrograms. Time, frequency, and amplitude distortions are modeled as smooth, invertible deformations, parameterized by scalar fields and applied via exponential maps. A neural network is trained to infer these fields from unpaired utterances of typical speech without using any pathological data. At test time, the model applies an approximate inversion near dysarthric inputs. Despite zero-shot generalization, we observe substantial ASR gains, including up to 16 percentage points WER reduction on challenging TORGO samples, with no degradation on clean speech. This work introduces a principled, interpretable approach for robust speech recognition under motor speech distortions.</p>
					<p>[2022-04-16] Automatic speech recognition (ASR) is crucial for human-machine interaction in diverse applications like conversational agents, household robots, call center automation, and automated subtitling. However, developing high-performance ASR models remains challenging, particularly for low-resource languages like Arabic, due to the scarcity of large, labeled speech datasets, which are costly and time-intensive to produce. In this work, we employ weakly supervised learning to train an Arabic ASR model using the Conformer architecture. Our model is trained from scratch on 13,000 hours of weakly annotated speech data covering both Modern Standard Arabic (MSA) and Dialectal Arabic (DA), eliminating the need for costly manual transcriptions. Despite the absence of human-verified labels, our approach attains state-of-the-art (SOTA) performance, exceeding all previous efforts in the field of Arabic ASR on the standard benchmarks. By demonstrating the effectiveness of weak supervision as a scalable, cost-effective alternative to traditional supervised approaches, paving the way for improved ASR systems in</p>

Figure 6: Comparison of image editing using the prompt “Please recreate the exact same image without any alterations.” with the original image. The original images contain blurred text that is not recognizable to humans. The rightmost column displays the OCR-extracted text from the original image using GPT-4o using the prompt “Directly output what is written in the image.”

### E.1 Image Reconstruction from Low-Quality Inputs

In this experiment, we provided GPT-4o with an intentionally degraded input image containing heavily distorted or unreadable text. Our prompt explicitly instructed the model to *recreate the image exactly without any alteration*. Interestingly, unlike diffusion-based models, which tend to replicate the visual noise and illegibility, GPT-4o instead produced an image where the text had been cleanly restored into readable, coherent sentences, as shown in Figure 6.

This behavior strongly deviates from the expected literal replication and instead suggests that GPT-4o engaged in a form of semantic hallucination. We hypothesize that GPT-4o first attempts to understand the image content through an internal representation, and in doing so, “fills in” the missing or noisy parts based on learned linguistic priors. To test this hypothesis, we queried GPT-4o to extract text from the original distorted image. Surprisingly, the model returned well-formed and highly plausible text, even though no readable characters are actually present in the image. Moreover, the extracted text closely matched the regenerated image, indicating a strong coupling between image understanding and generation.

These observations suggest that GPT-4o has inherited a strong capacity for image understanding. The model does not simply replicate noisy input, but instead attempts to semantically interpret and “restore” the image content, even when such interpretation involves hallucination. This behavior implies that GPT-4o’s backbone is not a generic image generation model, but one that possesses robust multimodal reasoning capabilities. We hypothesize that this capability arises either from: (1) **A shared autoregressive backbone** pretrained or co-trained for both language and vision tasks, enabling semantic-level image understanding and generation, or (2) **A language-centric model** (e.g., GPT-4) that has been subsequently fine-tuned on multimodal tasks, thereby acquiring the ability to parse and reconstruct image content via linguistic priors.

In either case, the consistency between the model’s interpretation and generation of text, despite degraded visual input, strongly supports the view that GPT-4o performs image generation not as a pixel-to-pixel transformation task, but as a language-informed semantic generation process.

### E.2 Text Addition and Deletion in Scene Context

To further explore GPT-4o’s ability to understand and manipulate visual content, we conducted a series of experiments focused on localized text editing – inserting and removing words from realistic visual scenes, such as blackboards and signage. These tasks require not only accurate prompt-following, but also semantic understanding of scene layout, font style, and background context.

In the text addition experiments, GPT-4o was prompted to insert specific phrases into designated regions of an image, as shown in Figure 7. The results show remarkable spatial precision and stylistic coherence: the added text matched the surrounding content in font, size, alignment, and even lighting and shading. In the deletion experiments, GPT-4o is instructed to remove certain words. Rather than

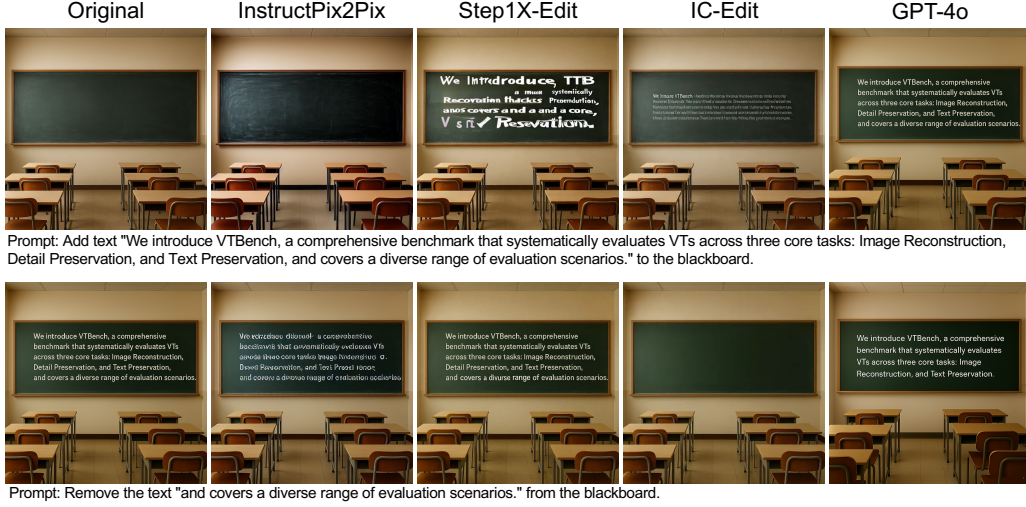


Figure 7: Text editing comparison across models, showing both text insertion (top) and removal (bottom) on a blackboard.

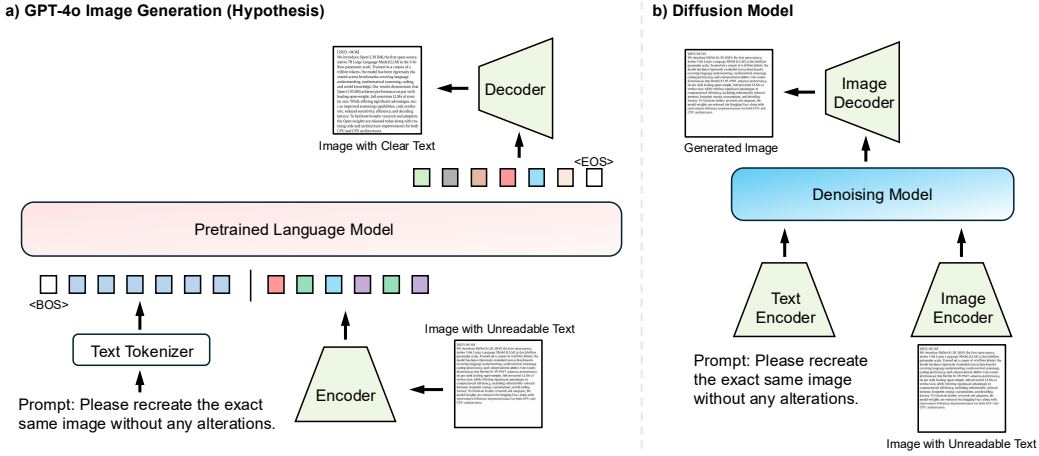


Figure 8: Comparison of two hypothesized architectures for image generation.

crudely masking out regions, the model naturally inpaint the background, reconstructing the texture and structure behind the deleted text with minimal artifacts.

These results reveal several important properties of GPT-4o’s architecture:

- **Semantic-level image editing:** The model does not simply manipulate pixels, but appears to operate at a higher level of abstraction. It understands which parts of the image correspond to the textual prompt and modifies them while preserving global visual coherence.
- **Language-conditioned spatial reasoning:** The edits are guided by natural language, which suggests a strong alignment between textual and visual representations. This is indicative of a shared or tightly coupled multimodal representation space.
- **Unified generation and understanding backbone:** The precision and fidelity of the edits, especially the seamless integration of new content, suggest that the same underlying autoregressive model is responsible for both interpreting the image and generating the modified output. This unified design contrasts with traditional pipelines that separate perception and generation.

Together with the hallucination behavior observed in the font reconstruction experiment, these findings support the view that GPT-4o integrates image understanding and image generation into a single, coherent process. It reasons about images in a way that is language-centric, and its visual tokenizer must be capable of encoding not only fine-grained appearance but also semantic structure and spatial context.

### E.3 Autoregressive vs. Diffusion: Implications for GPT-4.

As summarized in Figure 8, we hypothesize that GPT-4o adopts a unified autoregressive architecture rather than a diffusion-based pipeline. This hypothesis is supported by the following observations:

- **Semantic hallucination through language priors:** GPT-4o’s tendency to “restore” unreadable text into coherent language, despite prompts requesting exact replication suggests that its image understanding is conditioned by a language model prior. Such behavior is natural in an autoregressive framework where image and text tokens are processed in a shared sequence and jointly influenced by a pretrained language model.
- **Language-grounded editing and generation:** The model demonstrates precise text insertion and deletion aligned with natural language instructions, which requires not only generation capability but also deep semantic understanding of both visual context and instruction intent. This is hard to achieve in diffusion models, where the denoising model lacks linguistic grounding or token-level reasoning.
- **Modality reuse and efficiency:** The autoregressive formulation allows GPT-4o to reuse the same pretrained language model for both textual and visual reasoning, leveraging strong LLM priors for multimodal understanding. In contrast, diffusion models typically require separate encoders and decoders for each modality, making such deep integration more difficult.
- **Failure mode contrast:** Diffusion models tend to replicate noise patterns or preserve unreadability when asked to reconstruct degraded text, faithfully following low-level visual patterns. GPT-4o, on the other hand, produces semantically enriched outputs, even when that contradicts pixel-level fidelity, indicative of language-centric generation.

Together, these insights point toward GPT-4o employing an autoregressive backbone with a high-capacity visual tokenizer that supports semantic, instruction-driven generation. This structure allows GPT-4o to unify image understanding and image synthesis in a way that is tightly aligned with language modeling capabilities.

### E.4 GPT-4o’s Visual Tokenizer

Despite the impressive capabilities exhibited by GPT-4o in both image understanding and generation, its VT remains proprietary and undisclosed. Nevertheless, its behavior provides strong indirect evidence of a highly expressive VT design: it preserves fine-grained textual structure, aligns visual and linguistic semantics, and supports high-resolution, editable image representations. Unlike many existing discrete tokenizers that struggle with text reconstruction and spatial fidelity, GPT-4o’s VT appears to encode images in a way that is not only compact, but also semantically rich and compatible with AR decoding. To replicate such a VT, future work can prioritize three core capabilities:

- **High-fidelity image reconstruction:** The tokenizer should retain sufficient visual detail to allow accurate reconstruction of the input image, ideally matching the performance of state-of-the-art continuous VAEs in terms of perceptual quality and structure preservation.
- **Resolution scalability:** It should generalize across varying image sizes and support high-resolution inputs without introducing artifacts or requiring fixed input dimensions, a common limitation of many existing discrete tokenizers.
- **Compatibility with downstream language models:** The output token sequences must be structurally and semantically aligned with the expectations of LLMs, enabling seamless integration into autoregressive multimodal frameworks for joint reasoning and generation.

Architectures such as residual next-scale VAEs, hierarchical quantization, or continuous tokenization may serve as promising directions. Given the lack of public access to GPT-4o’s VT, benchmarks like VTBench offer a practical path forward: by systematically evaluating VT components in isolation, researchers can identify weaknesses, measure progress, and guide the development of open-source alternatives that approach or surpass GPT-4o’s performance.

## F Additional Visualize Qualitative Results

To complement the quantitative evaluations presented in the main paper, we provide additional qualitative results that illustrate the reconstruction quality, text preservation, and detail retention of various visual tokenizers, from Figure 9 to 13.

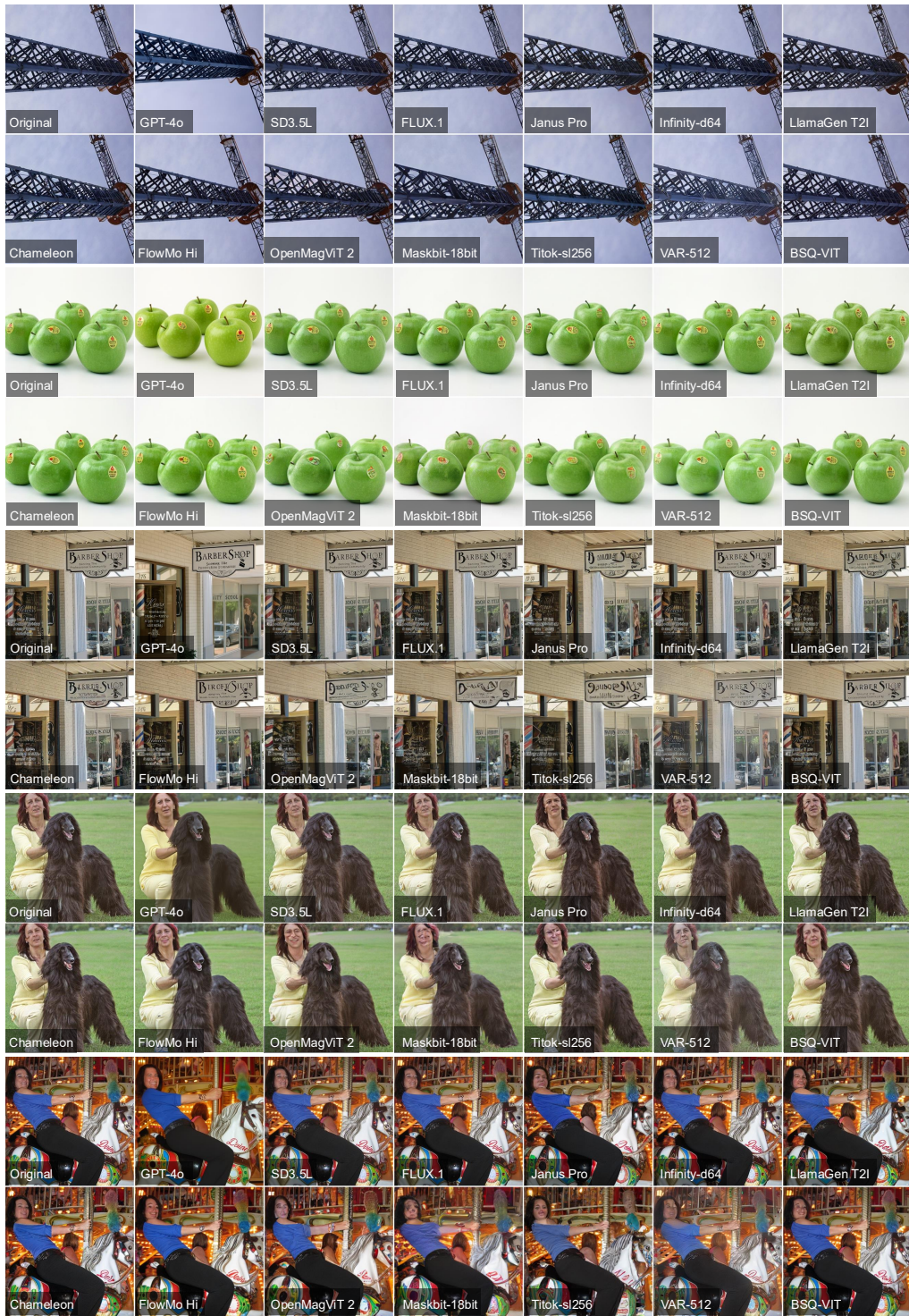


Figure 9: Additional visualize qualitative results for imagenet of task 1.

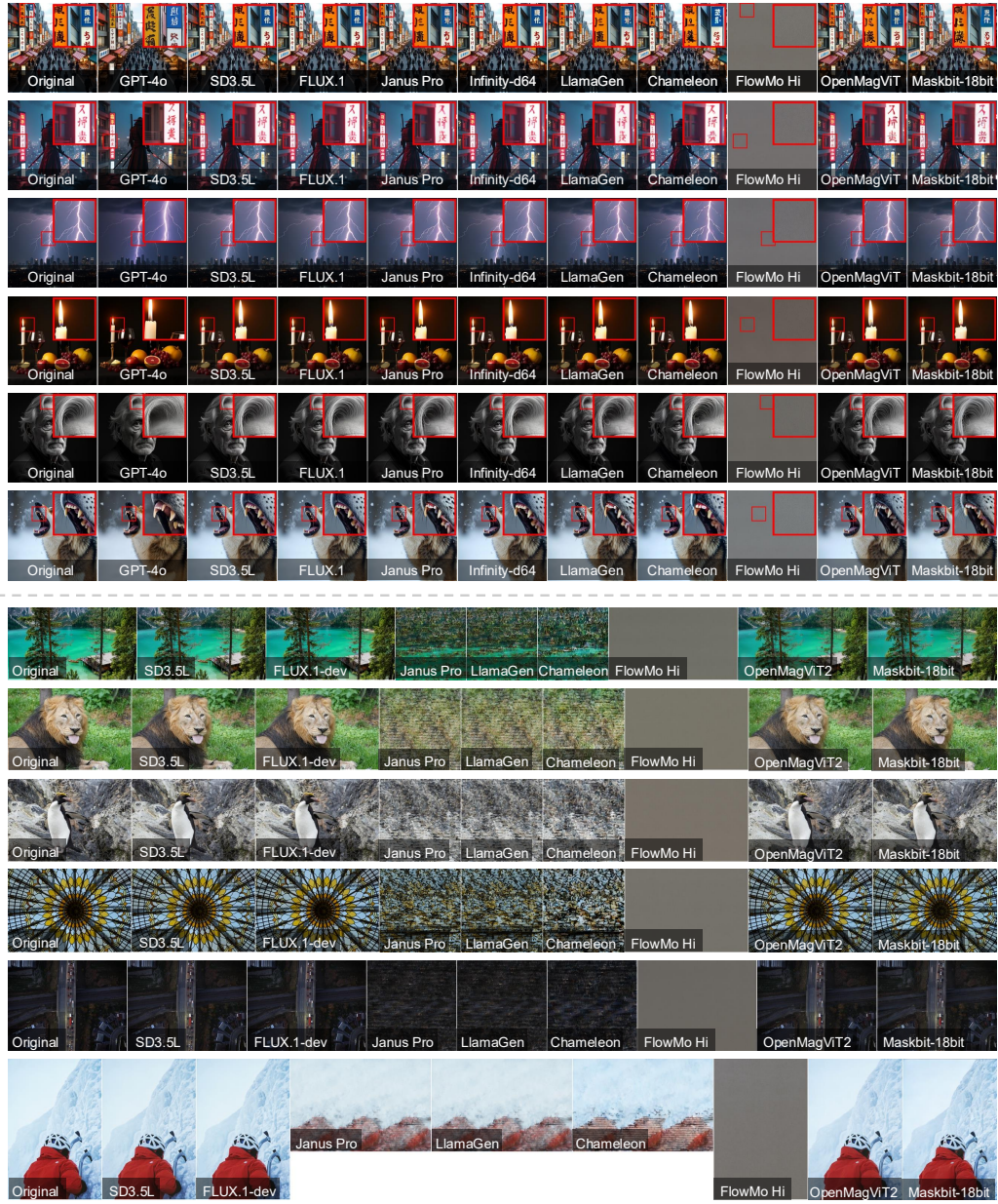


Figure 10: Visualized examples for high-resolution (top) and varying-resolution (bottom) of task 1.

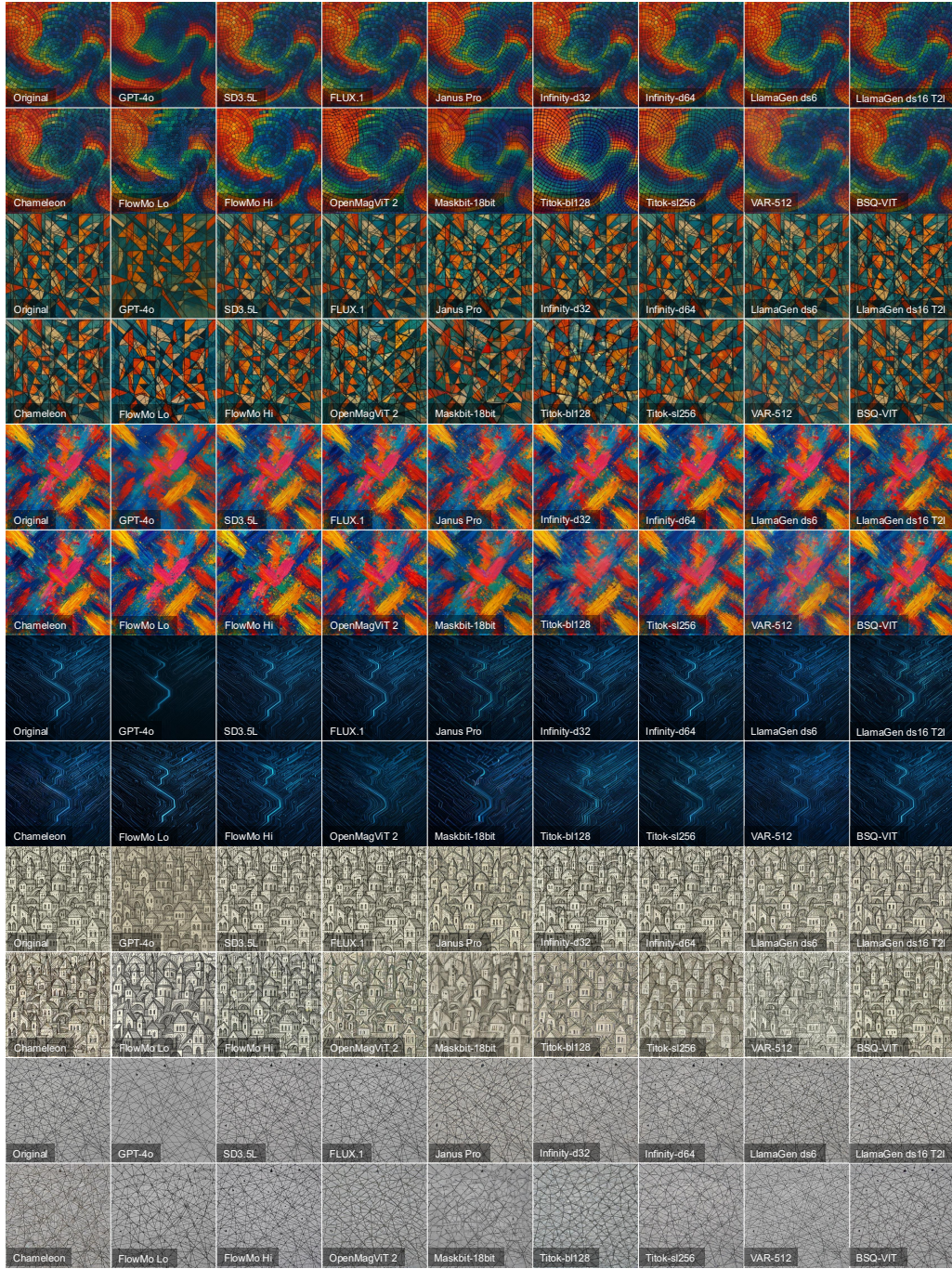


Figure 11: Additional visualize qualitative results for detail reservation (task 2).



Figure 12: Additional visualize qualitative results for movie posters of task 3. The corresponding model names are listed in the first row.

<p><b>Original</b></p> <p><b>Chameleon</b></p>	<p><b>GP1-4o</b></p> <p><b>FlowMo Lo</b></p>	<p><b>SD3 SL</b></p> <p><b>FlowMo Hi</b></p>	<p><b>FLUX.1</b></p> <p><b>OpenMagViT 2</b></p>	<p><b>Janus Pro</b></p> <p><b>Maskbit-18bit</b></p>	<p><b>Infinity-32</b></p> <p><b>TiTok-b128</b></p>	<p><b>Infinity-64</b></p> <p><b>TiTok-a1256</b></p>	<p><b>LlamaGen ds6</b></p> <p><b>VAR-512</b></p>	<p><b>LlamaGen ds16 T2</b></p> <p><b>BSQ-ViT</b></p>
<p><b>Original</b></p> <p><b>Chameleon</b></p>	<p><b>GP1-4o</b></p> <p><b>FlowMo Lo</b></p>	<p><b>SD3 SL</b></p> <p><b>FlowMo Hi</b></p>	<p><b>FLUX.1</b></p> <p><b>OpenMagViT 2</b></p>	<p><b>Janus Pro</b></p> <p><b>Maskbit-18bit</b></p>	<p><b>Infinity-32</b></p> <p><b>TiTok-b128</b></p>	<p><b>Infinity-64</b></p> <p><b>TiTok-a1256</b></p>	<p><b>LlamaGen ds6</b></p> <p><b>VAR-512</b></p>	<p><b>LlamaGen ds16 T2</b></p> <p><b>BSQ-ViT</b></p>
<p><b>Original</b></p> <p><b>Chameleon</b></p>	<p><b>GP1-4o</b></p> <p><b>FlowMo Lo</b></p>	<p><b>SD3 SL</b></p> <p><b>FlowMo Hi</b></p>	<p><b>FLUX.1</b></p> <p><b>OpenMagViT 2</b></p>	<p><b>Janus Pro</b></p> <p><b>Maskbit-18bit</b></p>	<p><b>Infinity-32</b></p> <p><b>TiTok-b128</b></p>	<p><b>Infinity-64</b></p> <p><b>TiTok-a1256</b></p>	<p><b>LlamaGen ds6</b></p> <p><b>VAR-512</b></p>	<p><b>LlamaGen ds16 T2</b></p> <p><b>BSQ-ViT</b></p>
<p><b>Original</b></p> <p><b>Chameleon</b></p>	<p><b>GP1-4o</b></p> <p><b>FlowMo Lo</b></p>	<p><b>SD3 SL</b></p> <p><b>FlowMo Hi</b></p>	<p><b>FLUX.1</b></p> <p><b>OpenMagViT 2</b></p>	<p><b>Janus Pro</b></p> <p><b>Maskbit-18bit</b></p>	<p><b>Infinity-32</b></p> <p><b>TiTok-b128</b></p>	<p><b>Infinity-64</b></p> <p><b>TiTok-a1256</b></p>	<p><b>LlamaGen ds6</b></p> <p><b>VAR-512</b></p>	<p><b>LlamaGen ds16 T2</b></p> <p><b>BSQ-ViT</b></p>

Figure 13: Additional qualitative results showing one ArXiv abstract and its corresponding multilingual versions (Chinese, Japanese, Korean, and Hindi) reconstructed by various visual tokenizers.